Deterministic error compensation for slow tool servo-driven diamond turning of freeform surface with nanometric form accuracy

Kodai Nagayama, Jiwang Yan *

Department of Mechanical Engineering, Faculty of Science and Technology, Keio University, 3-14-1 Hiyoshi, Kohoku-ku, Yokohama, 223-8522, Japan

ARTICLE INFO	ABSTRACT
	Slow tool servo (STS) turning takes an important role in fabrication of freeform optical elements. However, in conventional STS turning, it is technologically difficult to obtain nanometer-level form accuracy due to multiple error factors such as tool trajectory errors, tool alignment errors and dynamic follow-up errors of machine tools used. In this study, a deterministic process flow was proposed where all the main error factors were comprehensively analyzed, simulated and then compensated before machining based on the feedforward method, and the workpiece form error after compensation was predicted accurately. The proposed process flow enabled achieving nanometer-level form accuracy by a single cut without the necessity of repetitive trial-and-error. To demonstrate the effectiveness of the proposed method, cutting tests of a two-dimensional sine wave grid were attempted on single-crystal silicon and the proposed error compensation was applied. As a result, the form error was reduced to 8 nm P–V (peak to valley) with a surface roughness of 1 nm Sa by a single cut.

Introduction

Along with rapid advancement of optical science and information technology, the demands for freeform optical elements are becoming higher and higher to improve the performance and decrease the size of the optical systems. Freeform optics are used in a variety of fields such as photonics, virtual reality (VR), augmented reality (AR), autonomous cars, aerospace and biomedical imaging [1–3]. In the past a few years, the accuracy required for freeform optical lenses has been increasing from the sub-micrometer level to the nanometer level [4,5]. For machining such complicated freeform surfaces, ultraprecision diamond turning by using a slow tool servo (STS), which synchronizes the X- and Z-slide motions with C-axis rotation of a machine tool [6–10], is an effective solution. STS turning enables faster fabrication of freeform surfaces compared to conventional milling and fly cutting methods.

However, in STS turning, form errors are usually generated on the workpiece due to the complex machine kinetics compared with turning rotationally symmetric surfaces [11,12]. The coexistence of multiple error factors, such as tool trajectory errors, tool setting errors, and dynamic follow-up errors of machine tools, makes the problem very complicated [13–16]. There have been a few studies aiming to analyze and compensate these error factors. For examples, Neo et al. developed an analytical model for tool path generation in STS turning to evaluate

the tool trajectory errors between the generated tool trajectories and the ideal surfaces [17–19]. Gao et al. analyzed tool alignment errors toward X- and Y-axis and compensated tool nose radius errors in the machining of sinusoidal surfaces [20,21]. Yu et al. developed a tool path modification system to reduce the dynamic errors of machine tools [22,23]. Kim et al. analyzed control systems for tool servo turning by comparing a feedback control system with a feedforward control system to improve the tracking performance of machine tools [24].

Most of the previous researches focused on the effect of individual error factors and each error factor was compensated independently based on the feedback from the measurement of workpiece. As a result, error compensation was usually performed on a trial-and-error base. The cutting-measuring-compensating-cutting cycles had to be repeated for several times until achieving the required form accuracy, which is very time consuming. In addition, multiple test cuts cause an increase of cutting distance which leads to extra tool wear, especially when cutting hard brittle materials. The tool wear induces new error factors, which makes the compensation process more and more complicated and non-deterministic. Up to date, it is still technologically difficult to reduce the form errors down to the nanometer level by a single cut.

In this study, a feedforward based deterministic process flow is proposed for error compensation in STS turning, in which all the main error factors are comprehensively analyzed, simulated and compensated

* Corresponding author.
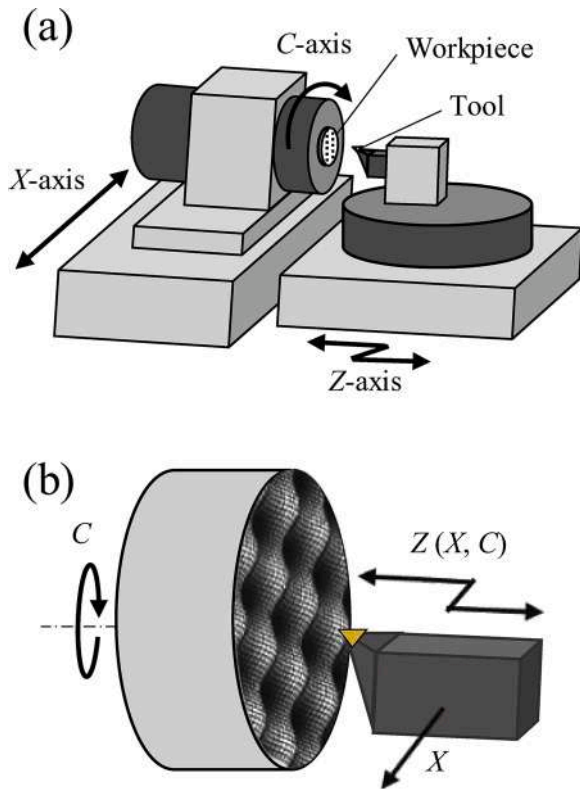*E-mail address:* yan@mech.keio.ac.jp (J. Yan).

Fig. 1. Schematic diagrams of (a) STS lathe structure and (b) STS turning of freeform surfaces.

before cutting to eliminate the need of multiple test cuts. The process flow consists three steps. First, modeling of the form error generation mechanism is performed for all the main error factors. Second, the relation between these error factors and the resulting workpiece form errors is analyzed and simulated. Third, based on the simulation results, all the error factors are compensated and the residual form error is predicted before the final machining step. To verify the effectiveness of the proposed process flow, fabrication tests of sinusoidal wave grids on single-crystal silicon are performed. The form errors of the machined surfaces are evaluated and compared with the predicted results to demonstrate the possibility of generating nanometer-level precision freeform surfaces on hard brittle materials.

Modeling and experimental procedures

Error factors in STS turning

Fig.1 (a) shows a schematic diagram of an ultraprecision lathe with an STS system. In STS turning, freeform surfaces are machined by synchronizing the X-/Z-axis movements with the C-axis rotation, as shown in Fig. 1(b). A typical STS turning process consists of three steps: programing step for tool path generation, tooling step for tool-workpiece alignment, and processing step for surface generation. Accordingly, major factors causing workpiece form errors during each step of the process are tool trajectory errors in the programing step, tool alignment errors in the tooling step, and dynamic follow-up errors of machine tools in the processing step [13–16]. These error factors can be further classified into many subcategories as listed in Fig. 2.

Error compensation method

Conventionally, form errors are compensated using a feedback method where each single error factor is compensated through a cutting-measuring-compensating-cutting cycle. This cycle must be repeated for several times until a form error within a required tolerance is achieved. This repetitive trial-and-error process is very time consuming, and multiple test cuts cause tool wear which makes the error compensation more and more difficult.
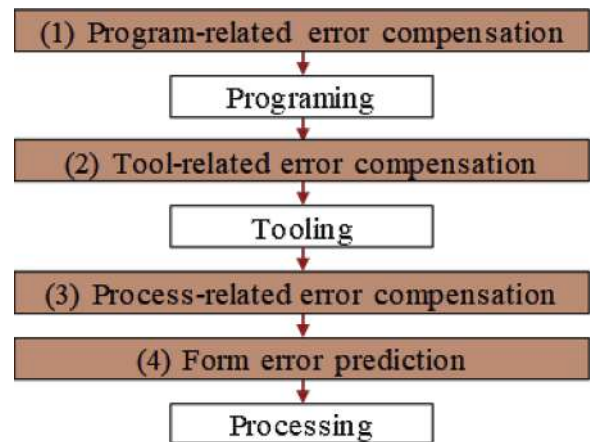

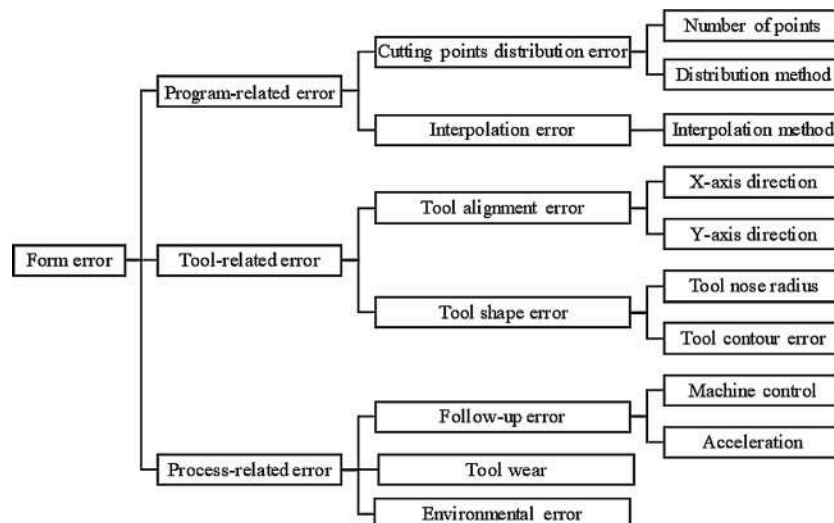**Fig. 3.** Classification of error factors in STS turning.

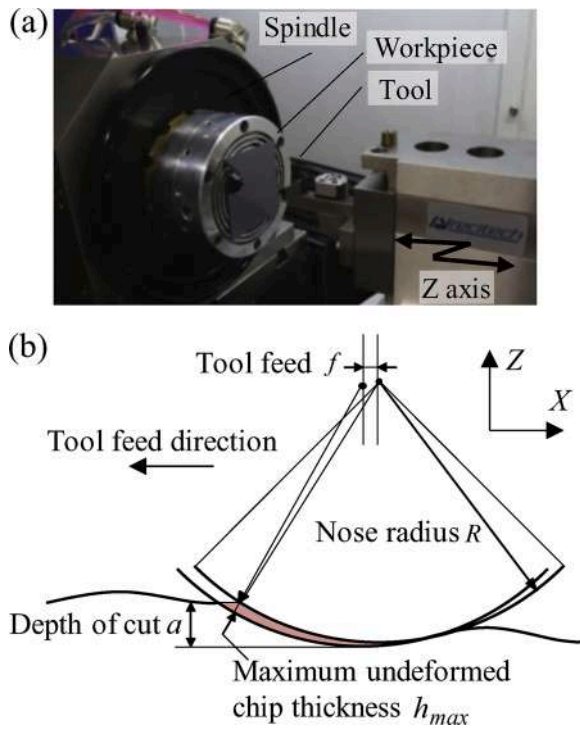**Fig. 2.** (a) Photograph of machining setup; (b) schematic cutting model.

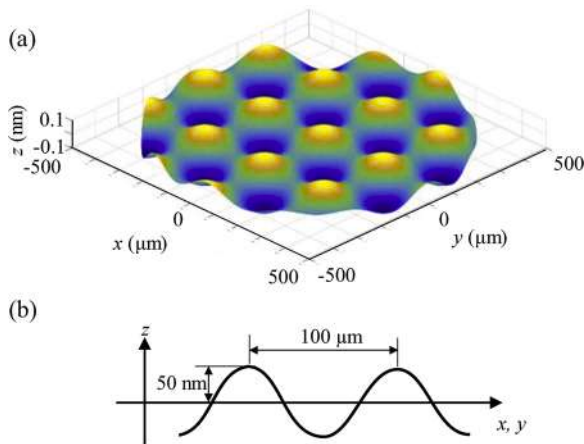**Fig. 4.** Proposed process flow for deterministic error compensation.

Fig. 5. Designed shape of workpiece surface: (a) three-dimensional topography, (b) cross-sectional profile at $y = 0$.

In this study, a feedforward based error compensation process flow was proposed as shown in Fig. 3, where the compensation of all main error factors is performed ahead of machining. The process is composed of four steps: (1) program-related error compensation, (2) tool-related error compensation, (3) process-related error compensation, and (4)

Table 1
Cutting conditions.

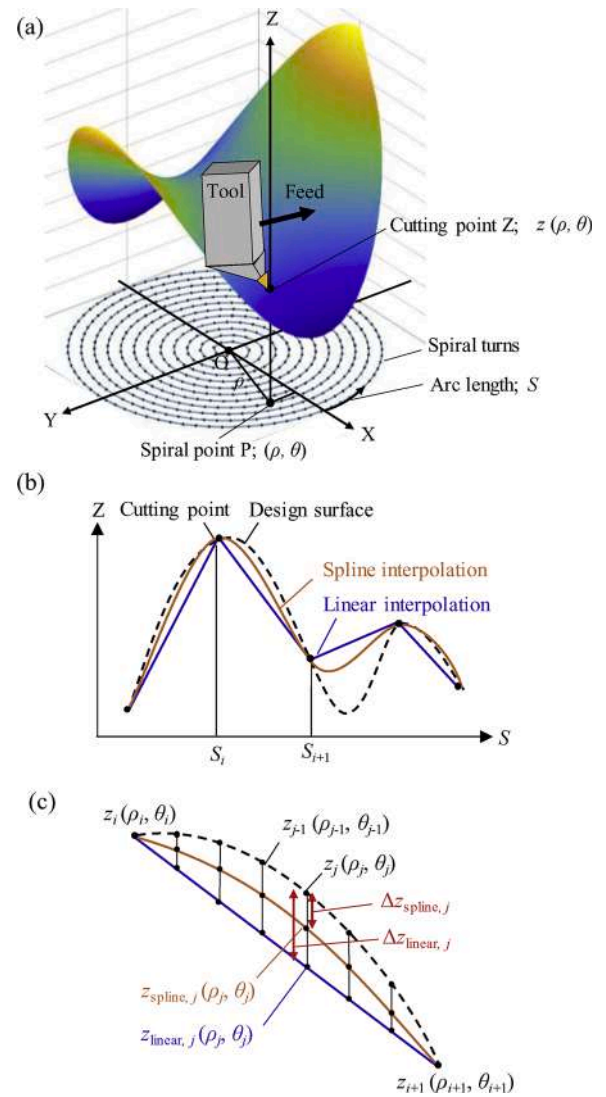| Cutting parameters	Values
Feed rate	2 μm/rev
Depth of cut	2.0 ~ 2.2 μm
Spindle rotation rate	20 rpm
Cutting tool	
Tool material	Single-crystal diamond
Nose radious	2 mm
Rake angle	$-30°$
Cutting atmosphere	Oil mist

Fig. 6. Schematic diagrams of (a) tool path generation in freeform surface turning, (b) interpolation of cutting points, and (c) simulation model of interpolation errors.

form error prediction. In this process flow, all the main error factors are compensated in steps (1)–(3) based on form error simulation without performing any test cuts. In step (4), the form error of the final workpiece surface is predicted and compared with the targeted tolerance. All the error compensation and prediction steps are carried out before machining, so that high form accuracy can be obtained by a single cut without the necessity of repeating trial-and-error test cuts and workpiece surface measurements. This will greatly save operation time and prevent extra tool wear before the final machining step. To realize the proposed process flow, theoretical modeling and experimental quantification of error factors was performed to establish the relations between the error factors and the resulting workpiece form errors.

Experimental method

To verify the effectiveness of the proposed process flow, cutting experiments were carried out by using different error compensation methods for comparison. An ultraprecision lathe Nanoform X produced by AMETEK Precitech Inc., USA, which has an STS system, was used. A photograph of the main section of the machining setup is shown in Fig. 4 (a). Fig. 4(b) is a schematic cutting model to describe the relationship among feed rate f, depth of cut a, tool nose radius R, and maximum
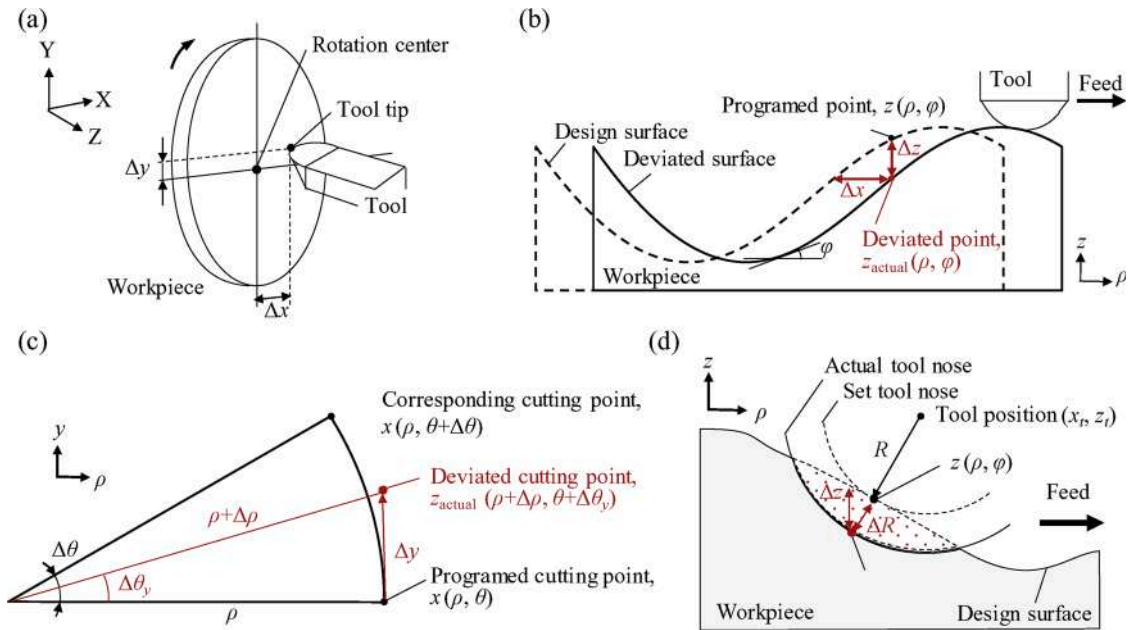
Fig. 7. Schematic diagrams of tool-related error factors: (a) tool alignment errors Δx and Δy, (b) influence of Δx, (c) influence of Δy, and (d) influence of tool radius error ΔR.
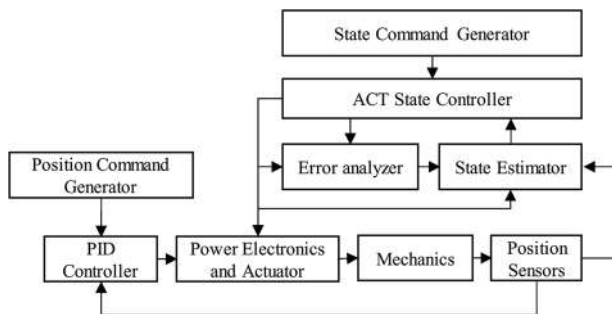

Fig. 8. Diagrams of the control system structure of the machine tool used.

undeformed chip thickness h_{max}. The value of h_{max} can be calculated by the following equation.

$$h_{max} = R - \sqrt{R^2 + f^2 - 2f\sqrt{2Ra - a^2}} \qquad (1)$$

As a typical free-form surface, a two-dimensional sine wave grid was designed and machined. The sine wave grid is described by the following equation.

$$z = A_1 \sin\left(\frac{2\pi}{\lambda_1}x\right) + A_2 \cos\left(\frac{2\pi}{\lambda_2}y\right) \qquad (2)$$

where A_1 and A_2 are amplitude in X axis and in Y axis, and λ_1 and λ_2 are wavelengths in X axis and in Y axis, respectively. In this study, A and λ were set to 50 nm and 100 μm, respectively. Fig. 5 shows the three-dimensional surface topography and cross-sectional profile of the targeted sine wave grid.

Two-dimensional sine wave grids can be used as surface displacement sensors [20]. For achieving a high resolution for the sensors, sub-micrometer or even ten-nanometer scale grid amplitude is required [21], where the form error is accordingly required to be much smaller, down to the nanometer level. However, methods for obtaining nanometer level form accuracy without trial-and-errors has not been established. Especially for STS turning of small-amplitude grids, the acceleration of machine tables is so high that it is difficult to prevent the follow-up error completely.

A single-crystal silicon (001) wafer was used as workpiece. A single-crystal diamond tool with a nose radius of 1.0 mm and a rake angle of -30° was used for cutting. A feed rate of 2 μm/rev and a depth of cut of 2.0~2.2 μm were used, leading to a maximum undeformed chip thickness of ~ 130 nm, according to Eq. (1). Under such a small undeformed chip thickness, ductile mode cutting can be realized in freeform surface turning of single-crystal silicon [12]. The cutting conditions are listed in Table 1. The surface topographies and cross-sectional profiles of the machined workpieces were measured by a white light interferometer Talysurf CCI 1000 (Taylor Hobson Ltd., UK). The final form errors were then calculated by fitting the measured profiles to the ideal surface geometry.

Modeling of error factors

Program-related error factors

In the programing step, a workpiece form error is caused by the deviation between a generated tool path and a designed surface. The tool path is generated by connecting corresponding cutting points on the designed surface, as shown in Fig. 6(a). In the cross section of X–Y plane, each cutting point is located on a spiral trajectory. Generally, the cutting points are distributed on the spiral trajectory through two different methods: Constant Angle (CA) method, where every angle between the corresponding cutting points is equal, and Constant Arc Length (CAL) method, where every arc length between the corresponding cutting points is equal [22,23]. As the pitch of two corresponding points decreases, the number of cutting points becomes larger, which decreases the form error, but increases the machining time.

The position of a specific point P on the spiral trajectory can be defined by the arc-length S, which is the length of the spiral trajectory from the spindle rotation center to the point P. This length S is given by the following equation:
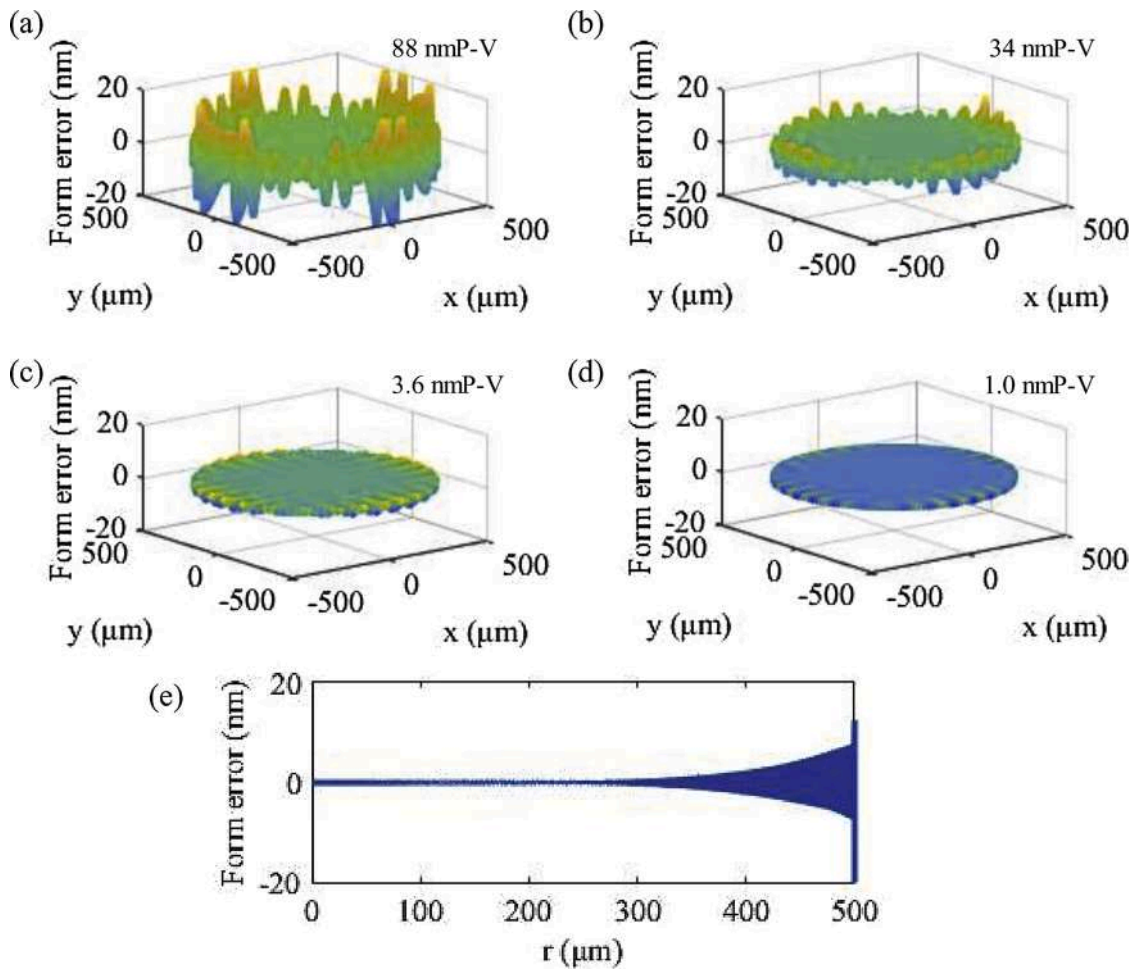
Fig. 9. Three-dimensional images of the calculated form errors in programing step with CA method: (a) $\Delta\theta = 5.0°$, (b) $\Delta\theta = 4.0°$, (c) $\Delta\theta = 3.0°$, (d) $\Delta\theta = 2.0°$; (e) is a two-dimensional profile when $\Delta\theta = 4.0°$.

$$S = \int \sqrt{\rho^2 + \left(\frac{d\rho}{d\theta}\right)^2}\, d\theta$$

$$= \frac{f_r}{2}\left[(2\pi N_t - \theta)\sqrt{(2\pi N_t - \theta)^2 + 1} + \ln\left|(2\pi N_t - \theta)\right.\right.$$

$$\left.\left. + \sqrt{(2\pi N_t - \theta)^2 + 1}\right|\right] \tag{3}$$

where ρ is the distance between the spindle rotation center O and the point P, θ is the total angle from the starting point of the spiral turns to the point P, f_r is the tool feed between the corresponding points, and N_t is the number of spiral turns. Each parameter is given by

$$\rho = r\text{-}f_r \cdot r \tag{4}$$

$$f_r = \frac{f}{2\pi} \tag{5}$$

$$N_t = \frac{r}{f} \tag{6}$$

where r is the workpiece radius and f is the pitch of the spiral turns, which is equal to the tool feed rate. S is then expressed as the function of θ. Finally, the cutting point Z can be obtained by substituting the point P into the function of a designed surface ($z(\rho,\theta)$).

The tool path is generated by interpolating the defined cutting points. There are two interpolation methods; linear interpolation and spline interpolation, as shown in Fig. 5 (b). In the programing step, a form error is caused on a machined surface due to a deviation between a designed surface and an interpolated tool path. However, the effect of the interpolation has not been considered in previous studies on STS turning [22,23]. To calculate the deviation, a line between any corresponding cutting points z_i and z_{i+1} is divided equally as shown in Fig. 5 (c). For linear interpolation, the slope between z_i and z_{i+1} is given by

$$\frac{dz_{linear,i}}{dS} = \frac{z_{i+1} - z_i}{S_i - S_{i+1}} \tag{7}$$

Then, a point on the linear-interpolated tool path ($z_{linear,\,j}$) can be expressed as follows.

$$z_{linear,j+1} = z_{line,j} + \frac{dz_{linear,i}}{dS}\, dS \tag{8}$$

On the other hand, for spline interpolation, a point on the spline-interpolated tool path ($z_{spline,\,j}$) is calculated by a function of cubic spline interpolation f as follows.

$$z_{spline,j} = f\left(z(\rho,\theta)\right) \tag{9}$$

Finally, the form error at a point on the designed surface (Δz) can be calculated by the following equations for both linear interpolation and spline interpolation.

$$\Delta z_{linear,j}(\rho_j, \theta_j) = z_{ideal,j}(\rho_j, \theta_j)\text{-}z_{linear,j}(\rho_j, \theta_j) \tag{10}$$

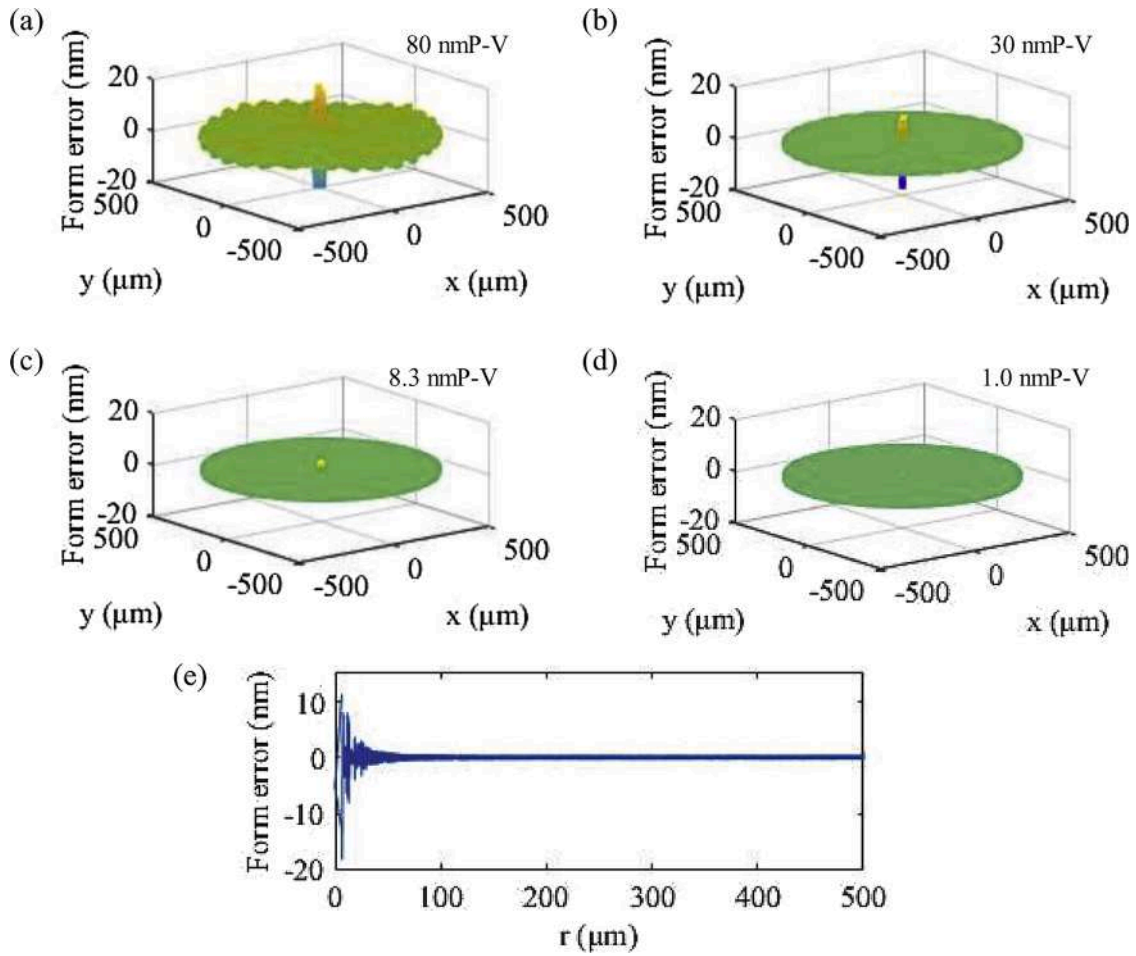$$\Delta z_{spline,j}(\rho_j, \theta_j) = z_{ideal,j}(\rho_j, \theta_j)\text{-}z_{spline,j}(\rho_j, \theta_j) \tag{11}$$

Fig. 10. Three-dimensional images of the calculated form errors in programing step with CAL method: (a) $\Delta S =30$ μm, (b) $\Delta S =20$ μm, (c) $\Delta S =10$ μm, (d) $\Delta S =5$ μm, (e) is a two-dimensional profile when $\Delta S =20$ μm.
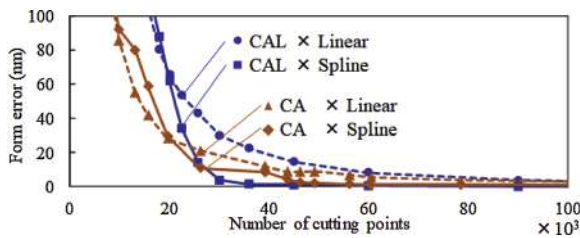

Fig. 11. Calculated form errors in relation to the number of cutting points with different distribution and interpolation methods.

Tool-related error factors

In diamond turning, the tool tip should be precisely aligned to the spindle rotation center. Otherwise, a workpiece form error is caused by the deviation. Fig. 7(a) presents a situation where the tool tip is aligned with an error Δx in X-axis and another error Δy in Y-axis. Fig. 7(b) presents a model for the influence of Δx in the cross section on X–Z plane of the designed surface. An actual tool cutting position is shifted from an ideal cutting point by Δx, which causes the form error on the machined surface. The error in Z-axis (Δz_x) at a deviated tool position is given by

$$\Delta z_x(\rho,\varphi) = z_{actual}(\rho,\varphi) - z(\rho,\varphi) = -\Delta x \cdot \tan\varphi \tag{12}$$

$$\tan\varphi = \frac{\partial z(\rho,\varphi)}{\partial \rho} \tag{13}$$

where ρ is the radius from the spindle rotation center to the cutting point and φ is the slope of the designed surface at a cutting point. Fig. 7(c) shows a model for the influence of Δy in the cross section on X–Y plane of the designed surface. The deviated tool position z_{actual} is represented as

$$z_{actual}(\rho,\theta) = z(\rho - \Delta\rho, \theta - \Delta\theta_y) \tag{14}$$

where $\Delta\rho$ and $\Delta\theta_y$ are the errors of ρ and θ, respectively, which are given by the following equations.

$$\Delta\rho = \rho\left(\sqrt{1 + \left(\frac{\Delta y}{\rho}\right)^2} - 1\right) \tag{15}$$

$$\Delta\theta_y = \tan^{-1}\left(\frac{\Delta y}{\rho}\right) \tag{16}$$

Finally, the form error in Z-axis (Δz_y) at a cutting point can be calculated as follows.

$$\Delta z_y(\rho,\theta) = z_{actual}(\rho,\theta) - z(\rho,\theta) \tag{17}$$

In addition to the tool alignment errors Δx and Δy, a tool shape error also causes a form error. As shown in Fig. 7(d), the tool position (x_t, z_t) is calculated for each cutting point with a tool nose radius R, which is given by the following equations.

$$x_t = x - R \cdot \sin\varphi \tag{18}$$
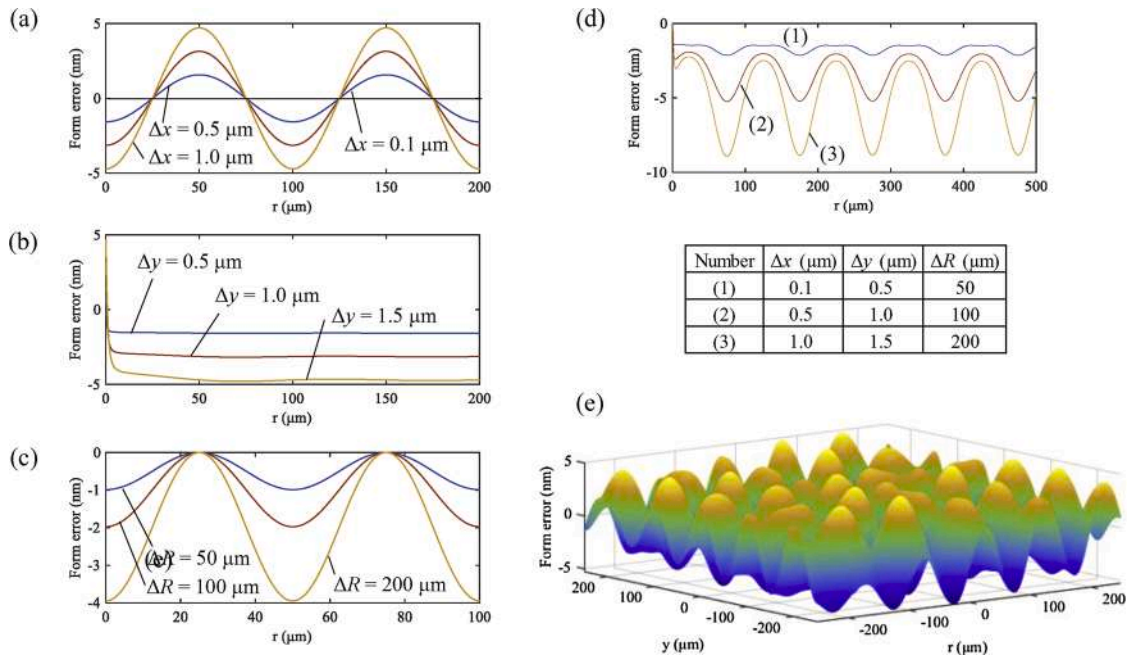
$$z_t = z - R \cdot \cos\varphi \tag{19}$$

Fig. 12. Profiles of the calculated form errors in XZ plane with different error factors: (a) Δx, (b) Δy, (c) ΔR; (d) is the profiles of the calculated form errors considering all the tool-related errors; (e) is three-dimensional image of the calculated form error when (Δx, Δy, ΔR) = (0.5, 1.0, 100).

Table 2
Control parameters used in PID.

Control parameters		Axis		
		x	z	c
No. 1	Kp	60	100	70
	Ki	7000	7000	7000
	Kd	0.9	1.2	0.7
No. 2	Kp	110	180	100
	Ki	10,000	10,000	10,000
	Kd	1.1	1.5	1.5

Table 3
Control parameters used in ATC.

Control parameters		Axis		
		x	z	c
No. 1	System BW	12	12	10
	M	1	1	0.115
	ACC FF	0	0.0009	0
No. 2	System BW	15	16	8
	M	4	4.8	0.3
	ACC FF	0.001	0.001	0

Even a tool is fabricated at extremely high precision, it has an error of nose radius ΔR. As a result, the tool edge is slightly deviated from a designed surface, which causes the form error. In this case, the form error at a cutting point Δz_R can be calculated as

$$\Delta z_R(\rho, \varphi) = -\Delta R\left(\frac{1}{\cos\varphi}-1\right) \qquad (20)$$

Process-related error factors

In the processing step, a workpiece form error is caused by the follow-up errors of the machine tool used. Due to the high acceleration of machine tables during tool oscillation, the tool movement is deviated from a programed tool path, especially at a cutting point where the

acceleration is large. The follow-up error is significantly influenced by the machine control systems. To solve this problem, some previous studies attempted to add an extra control system to a standard machine controller or to establish a method for cancelling the follow-up error by theoretical modeling of the machine control system [22–24]. However, these methods made the control system very complicated, and sometimes unstable.

In this study, we focused on gains of the standard control system of the machine. To decrease the follow-up error, we attempted to adjust the gains according to the designed surface and cutting parameters rather than fixing the gains. This method is simple, and valid for all the machines regardless of the control system types. As an example, a system block diagram of the ultraprecision lathe used in this study is shown in Fig. 8. The system, which is called ACT (Adaptive Control), is composed of a feedback system and a feedforward system [25,26]. In the feedback system, output u(t) from input e(t) is expressed by following equation.

$$u(t) = K_p e(t) + K_i \int_0^t e(\tau)d\tau + K_d\frac{de(t)}{dt} \qquad (21)$$

where K_p is a proportional gain, K_i is an integral gain and K_d is a differential gain. The ACT system suppresses follow-up errors by predicting the errors ahead of tool movements during machining. Although the details of the ACT system are not revealed, three main parameters (System Band Width: System BW; M; and Acceleration feedforward; ACC) are available for control use by the operator. System BW is the gain of the whole ACT system, which determines the strength of the ACT control. M is the parameter corresponding to the weight of each machine axis, which is used for predicting inertia of machine movements. ACCFF is the parameter suppressing an over acceleration.

Form error quantification

Program-related form error generation

Form errors were calculated using different distribution methods, interpolation methods and number of cutting points. Fig. 9 shows three- and two-dimensional distributions of the calculated form errors when the tool path was generated by Constant Angle (CA) method with
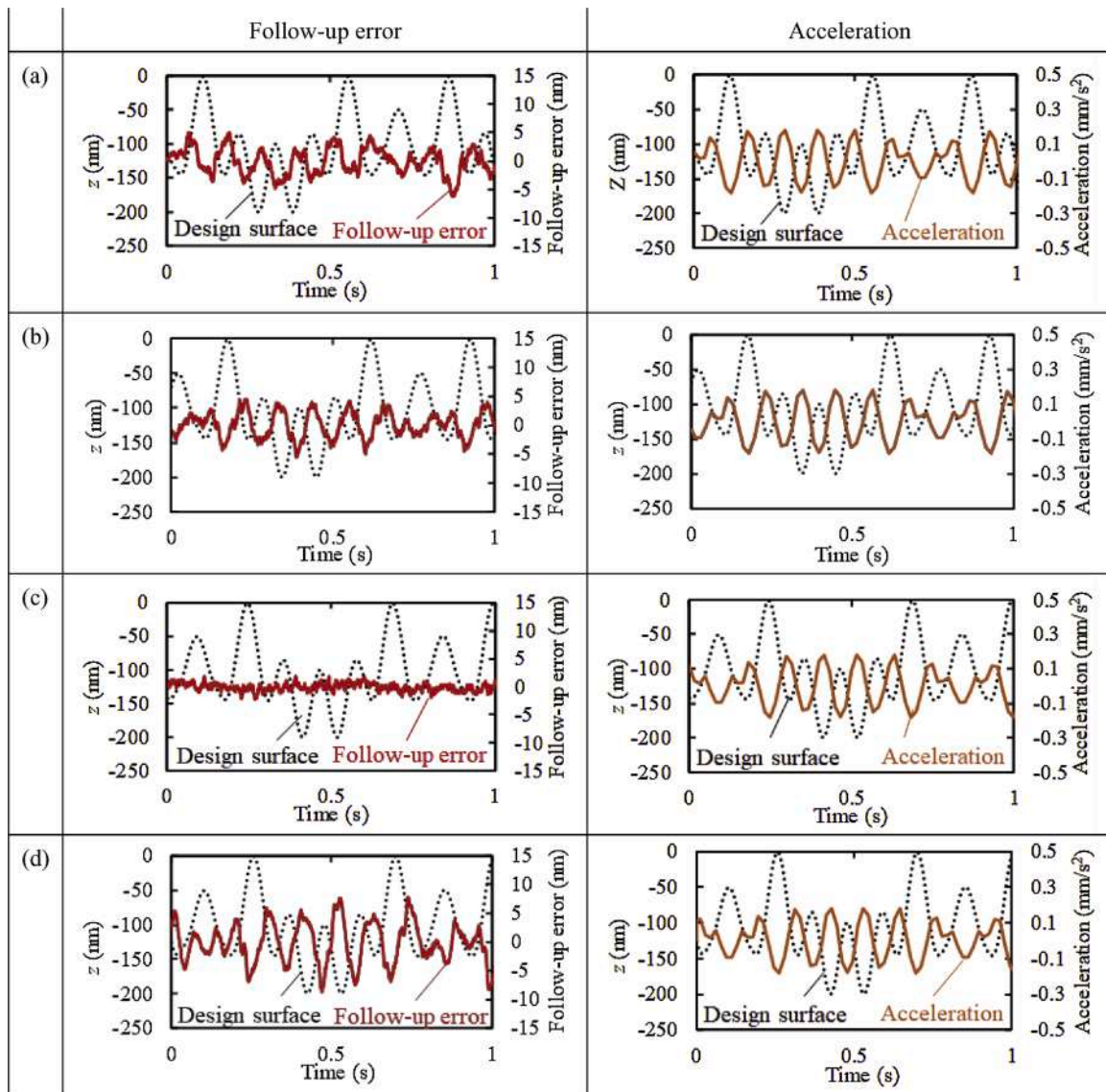
Fig. 13. Measurement results of follow-up error and acceleration of Z-axis: (a) PID, (Kp, Ki, Kd) = (180, 10,000, 1.5); (b) PID, (Kp, Ki, Kd) = (100, 7000, 1.2); (c) ATC, (System BW, M, ACCFF) = (16, 3.8, 0.001); (d) ATC, (System BW, M, ACCFF) = (12, 4.0, 0.0009).

different $\Delta\theta$ and linear interpolation. It is obvious that a smaller $\Delta\theta$ decreased the form error as increasing the number of cutting points. As shown in the two-dimensional profile of the calculated form error when $\Delta\theta = 4.0°$ (Fig. 9(e)), the form error gradually decreased from the outer area of workpiece toward the workpiece center. This phenomenon was caused by the change of intervals between corresponding cutting points, as described in a previous study [17]. Since $\Delta\theta$ is constant in CA, the intervals became smaller in the inner part of workpiece as the distribution of the cutting points becoming denser. As a result, the deviation between the interpolated tool path and the designed surface, which is equal to the form error, decreased.

The three- and two-dimensional distributions of the calculated form errors by CAL method with different ΔS are shown in Fig. 10. Similar to the results of CA, the form error was smaller at a smaller interval ΔS. As shown by the two-dimensional profile of the calculated form error when ΔS =20 μm (Fig. 10(e)), the form error dramatically increased near the workpiece center. This phenomenon seems to be caused by an increase of $\Delta\theta$ at the inner part of the workpiece which made the distribution of the cutting points sparse, since ΔS is constant for any corresponding points in the CAL method.

The form errors in relation to the number of cutting points for different distribution and interpolation methods are summarized in Fig. 11. For most conditions, the form errors were smaller in CA than in CAL. This is due to the dramatic increase of form errors at the workpiece center in CAL as shown in Fig.10(e). It is also found that a superiority or inferiority between spline interpolation and linear interpolation was changed depending on the number of cutting points. Linear interpolation resulted in the smaller form error at the smaller number of cutting points, whereas spline interpolation achieved the smaller form error at the larger number of cutting points. These simulation results enable to modify the program parameters to satisfy the targeted tolerance in a minimum machining time.

Tool-related form error generation

Fig. 12 shows the simulation results of tool-related form error generation. Fig. 12(a) and (b) show profiles of the calculated form errors in X–Z plane with different alignment errors Δx and Δy. It is obvious that the form error becomes larger with the larger amount of alignment errors and that the influence of Δy is as large as that of Δx. Fig. 12 (c) shows profiles of the calculated from errors in X–Z plane with different ΔR. Since the form error is actually caused by all the above-mentioned
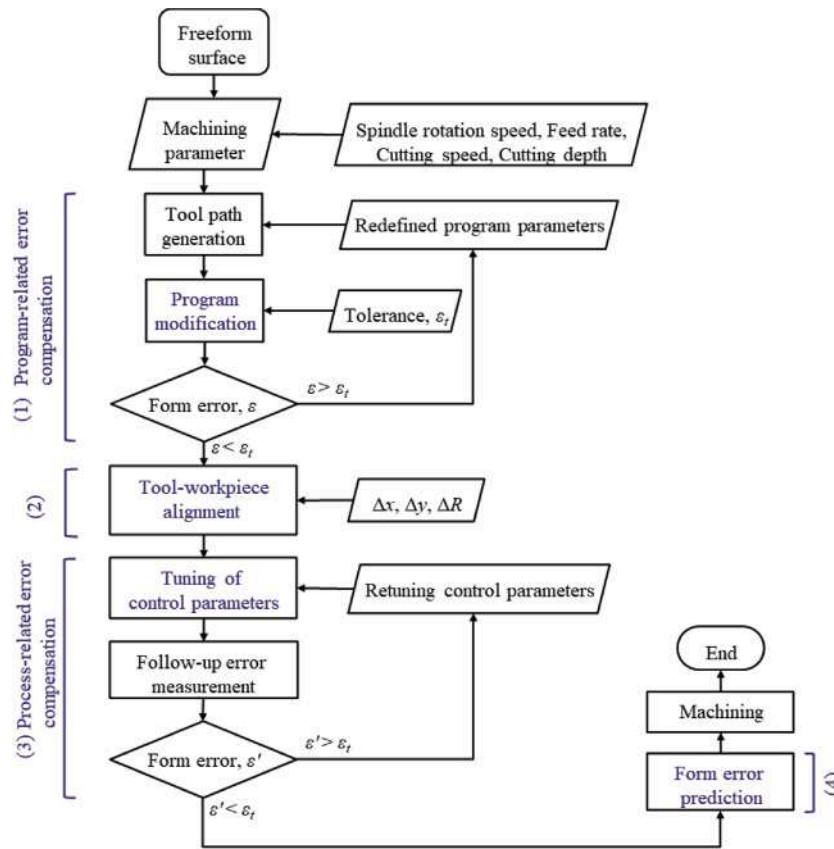
Fig. 14. Flowchart of the proposed compensation method.

Table 4
Program parameters before and after modification.

Program parameters	Values	
	Before	After
Interpolation method	Spline	Spline
Cutting points distribution	CAL	CA
Number of cutting points	13,090	45,000

Table 5
Tool-related errors before and after tool-workpiece alignment.

Error parameters	Values	
	Before	After
Δx (μm)	−3.5	−0.25
Δy (μm)	−3.5	−0.25
ΔR (μm)	100	10

Table 6
Control parameters before and after tuning.

Control parameters		Before			After		
		Axis			Axis		
		x	z	c	x	z	c
PID	Kp	60	100	70	110	180	100
	Ki	7000	7000	7000	10,000	10,000	10,000
	Kd	0.9	1.2	0.7	1.1	1.5	1.5
ATC	System BW	12	12	10	1.5	16	8
	M	4	4	0.115	4	4.8	0.3
	ACCFF	0	0.0009	0	0.001	0.001	0

error factors, the form error due to all the tool-related error factors was calculated as shown in Fig. 12(d). Fig. 12(e) shows a three-dimensional image of the calculated form error when Δx, Δy and ΔR are 0.5 μm, 1.5 μm and 100 μm, respectively. These simulations enable to quantitatively predict the form error in the tooling step to make a criterion of required alignment accuracy.

Process-related form error generation

Follow-up errors in axes Z, X and C were measured with different control parameters with the PID and ATC methods, respectively. The PID parameters set for all the axes are shown in Table 2. In the PID control, K_p, K_i and K_d were changed by steps of 10, 1000 and 0.1. when $60 < K_p <190$, $6000 < K_i < 11,000$ and $1.1 < K_d < 1.6$, the follow-up error was suppressed below a specific value and was the minimum when $K_p = 180$, $K_i = 10,000$ and $K_d = 1.5$. For parameters beyond the ranges of $60 < K_p <190$, $6000 < K_i < 11,000$ and $1.1 < K_d < 1.6$, the machine axis follow-up error was not attenuated so that oscillation of the axis was detected. This is because the gain input was too small to control the machine movement, or the gain was so large that the follow-up error was conversely amplified. The ATC parameters set for all the axes are shown in Table 3. In the ATC method, we changed system BW in the range of 12 ~ 16 by a step of 0.1, where the oscillation of axes did not occur. M was changed by a step of 0.1 in the range of 3.5 ~ 4.5. Under these conditions, ACCFF was increased by a step of 0.1 from 0.

The measurement results of the follow-up errors and corresponding accelerations with these parameters are shown in Fig. 13. Since the relation between the control parameters and the follow-up errors were quite similar among all the axes, the results are shown only for Z axis in the following discussion. In both Fig. 13(a) and (b), the follow-up errors are higher around the peaks and valleys of the tool paths. This is because the acceleration becomes dramatically higher at those points. There is
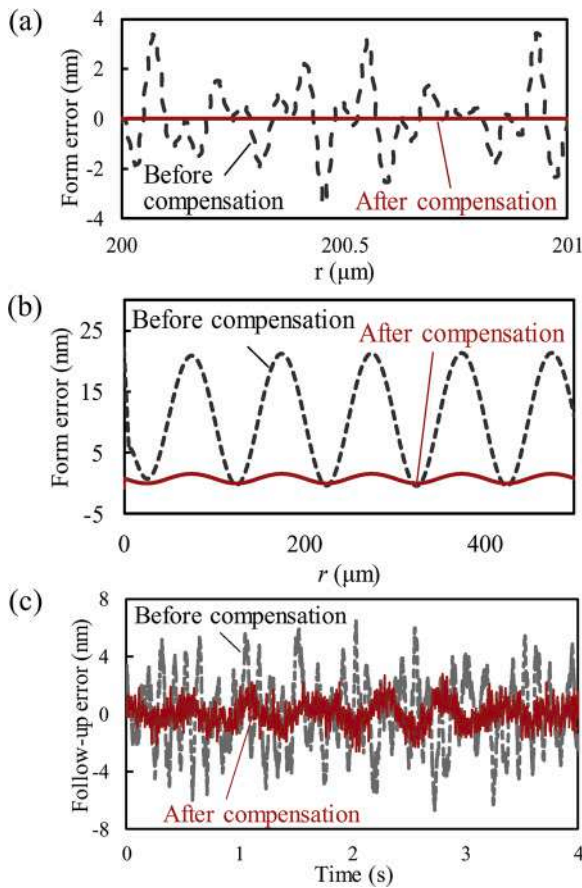
Fig. 15. Profiles of the calculated form errors before and after (a) program modification, (b) tool-workpiece alignment, and (c) tuning of control parameters.
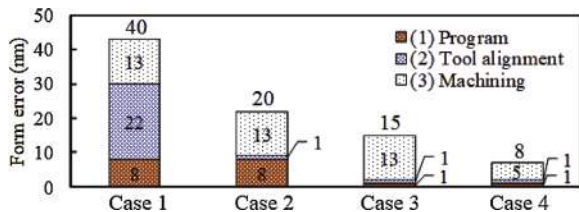

Fig. 16. Prediction results of the form errors in different compensation conditions.

no significant difference of the acceleration in Fig. 13(a) and (b) regardless of the control parameters. However, the comparison shows that the follow-up error is more suppressed when using the larger gains. It indicates that tuning the gains can decrease follow-up errors even for the same acceleration of tool movements. If the gain was increased a little more than the modified parameters, the divergence easily occurred. Therefore, in the tuning of the PID control gains, the gains should be set as large as possible unless the divergence occurs for minimizing the follow-up errors.

In Fig. 13(c), the form error became minimum when System BW, M and ACCFF were 16, 3.8 and 0.001. The follow-up error when System BW, M and ACCFF were 12, 4, 0.0009, as shown in Fig. 13(d). Since System BW takes a role like a gain of the PID, it is effective to set System BW as large as possible, as described above. Since M represents the weight of machine axes, it should be adjusted to a current setup of each axis one by one as checking the output of follow-up error. In this experiment, the weight of the current axis seemed to be less because the

follow-up error was smaller with a smaller amount of M. Since ACCFF depends on machining procedures such as a surface design and a machining speed, it would be the best to modify ACCFF after the other two gains were set.

From comparison of Fig. 13(a) and (d), it is demonstrated that the ATC is not always more effective than the PID to suppress the follow-up error. On the other hand, comparison of Fig. 13(a) and (c) indicates that after tuning the parameters properly, the follow-up error was decreased by a half using the ATC. This shows the effectiveness of the ATC control, which predicts and decreases the follow-up error ahead of input. It can also be said that tuning of the control parameters against every cutting condition is highly effective to decrease the follow-up error. This has not been realized by previous studies where the parameters were set constant.

Error compensation

Compensation flow

Based on the form error quantification results, an error compensation flow was proposed as shown in Fig. 14. The main steps include:

(1) A tool path is generated for a designed freeform surface, and a form error caused by the program-related error is then calculated. If the form error is above the targeted tolerance, the programming parameters are modified.
(2) A tolerance of the tool-related error is set before the tooling step. Tooling is carried out to make the resulting workpiece form error less than the tolerance.
(3) Tuning of control parameters are performed and a follow-up error is experimentally measured. If the measured follow-up error satisfies the tolerance, a tool path is finally generated.
(4) The residual workpiece form error is predicted before machining based on the results of steps (1) - (3). Not only the total amount of form error but also the fractions of each error factor is visualized, which provides suggestions for further improvement of form accuracy.

To verify the effect of each error compensation step, the following case study was carried out for comparison:

Case 1: without error compensation
Case 2: with compensation of tool-related error
Case 3: with compensations of tool-related error and program-related error
Case 4: with compensations of tool-related error, program-related error and process-related error

Table 4 shows the program parameters, including the interpolation methods, the distribution methods and the number of cutting points, before and after the program modification. Table 5 shows the tool-related errors before and after the tool-workpiece alignment. Table 6 shows the machine control parameters before and after the tuning of control parameters. In this study, the target tolerance was set to 1 nm P–V in each compensation step.

Case comparison

Fig. 15 shows profiles of the calculated form errors before and after program modification, tool-workpiece alignment, and tuning of control parameters, respectively. As seen in Fig. 15(a), by increasing the number of cutting points by 2.5 times, the form error was decreased from 8 nm to 1 nm P–V. Due to the increase of cutting points, the machining time was increased by 10 min. For tool alignment, Δx and Δy were required to be under 0.25 μm, and ΔR under 10 μm to achieve the tolerance of 1 nm P–V, as shown in Fig. 15(b). In Fig. 15(c), measurements of the follow-up errors were performed for 4 s from the position of $(x, y) = (100, 0)$. The form error was decreased from 13 nm to 5 nm P–V, especially in the
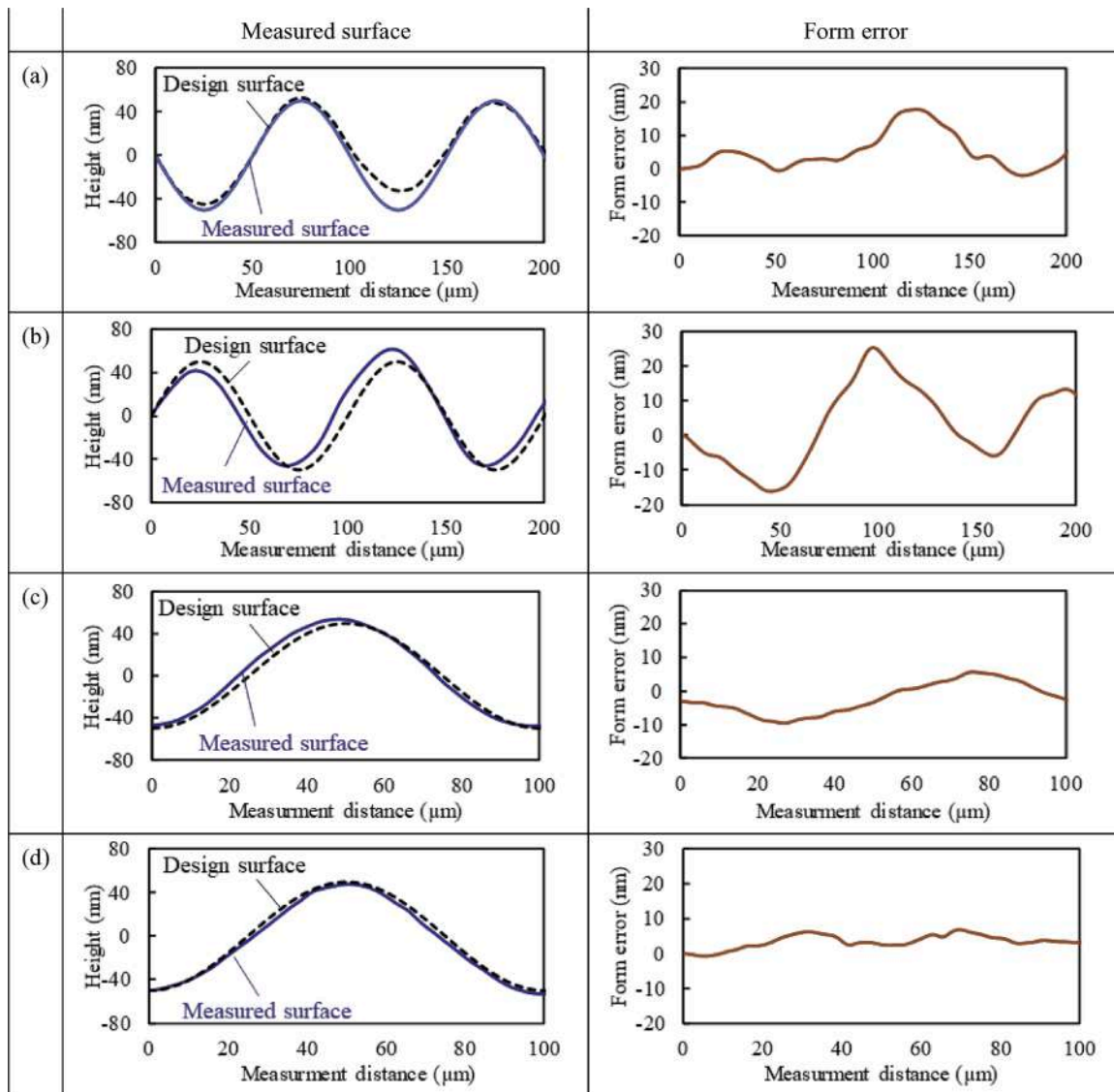
Fig. 17. Profiles of the measured surfaces and form errors in (a) Case 1, (b) Case 2, (c) Case 3, and (d) Case 4.
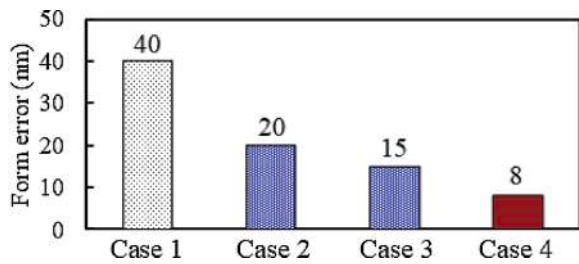

Fig. 18. Measurement results of the form errors in different compensation cases.

Fig. 19. Three-dimensional image of machined nanometer scaled sine wave grid on single-crystal silicon (Case 4).

peaks of the tool path, where the tool's acceleration seemed to be larger. This is because a high gain has applied a proper amount of feedback to the cutting tool movement to cancel the disturbance of the acceleration. However, after the tuning, a small noise was detected on the measured profile. This is because the feedback was excessively applied toward small changes of the acceleration to cause a sort of tool vibration. If the gain is excessively high, a divergence occurs, as mentioned in Section 4.3. In the tuning of the PID control parameters, the gain should be set as large as possible for minimizing the follow-up errors unless the
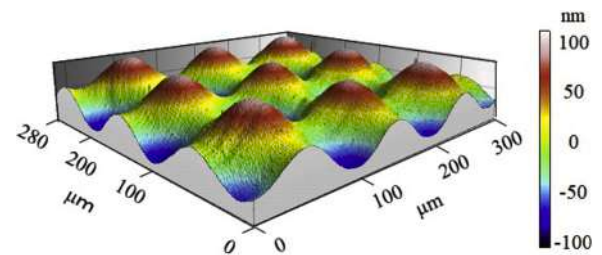
divergence occurs.

Prediction of residual form error

Fig. 16 shows the predicted results of residual form errors after each error compensation step. Without error compensation (Case 1), tool alignment is the dominant error factor. By adding the compensation steps, the form error was decreased gradually from Case 1–4. Each error compensation step successfully suppressed the form error generated in
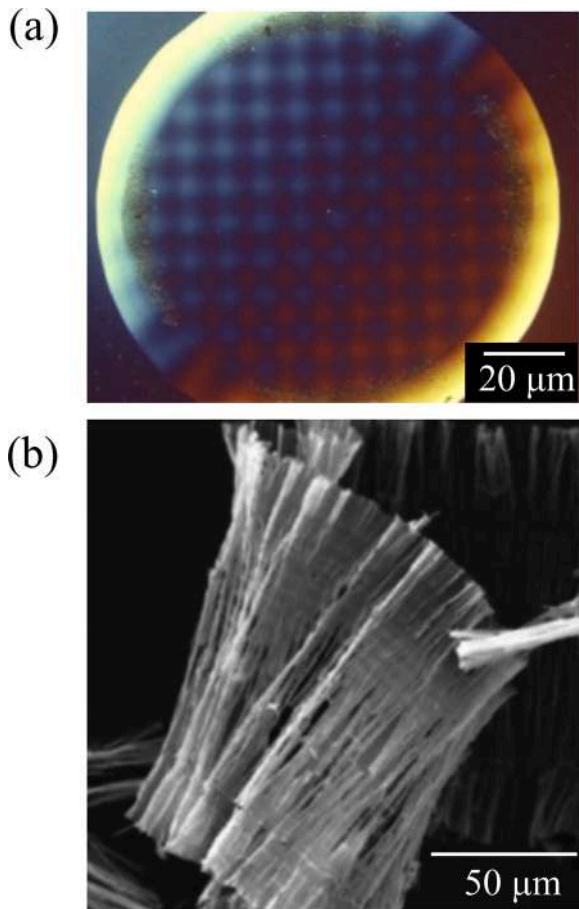
Fig. 20. (a) Microscope image of the machined two-dimensional sine wave grid on single-crystal silicon and (b) SEM image of ductile-cut chips.

the same step. However, in the conventional compensation flow where only a single error factor is considered, like Case 2, a big residual form error exists, and thus additional machining cycles are still required. On the other hand, in the proposed compensation flow where all the error factors are comprehensively compensated, i.e., Case 4, all the error factors are suppressed so that high form accuracy can be obtained in a single cut. In this study, it was predicted that the form error was less than 10 nm P–V for the sine wave grid.

Experimental verification and discussion

Finally, machining experiments were performed to verify the effectiveness of the proposed error compensation flow. The cutting conditions are shown in Table 1, and the conditions for each compensation step are shown in Tables 4–6. The measured surface profiles and the form errors for Cases 1–4 are shown in Fig. 17. The measurements were performed at a fixed location ($\theta = 0°$, $r = 250$ μm) on the workpiece. Since the distribution of form error is independent of direction [22], the form error evaluation in this study was carried out only along the direction of $\theta = 0°$.

In Case 1, the measured profile is significantly deviated from the ideal surface, which shows a form error of 40 μm (Fig.17(a)). In Case 2 (Fig.17(b)), after the tool-workpiece alignment, the form error decreases to 20 μm, which agrees well with the predicted result in Fig. 16. In Case 3, the form error is slightly decreased, however, around the peaks and valleys of the sine wave, significant deviation along with Z direction still remains (Fig. 17(c)). This is because the follow-up error easily occurs in these areas. In Case 4, however, all the error factors are compensated successfully (Fig. 17(d)). The measured surface fits well with the ideal

surface.

The measurement results of the residual form errors in Cases 1–4 are shown in Fig. 18. The form error of Case 4 is 8 nm P–V, demonstrating that the form error in STS turning can be decreased to the nanometer level by compensating all the error factors before machining. Moreover, a comparison between Figs. 16 and 18 shows that the predicted result agrees well with the experimental result. This fact demonstrates that the proposed models of form error generation are correct and can be used to precisely predict the final form error ahead of machining.

Fig. 19 is a three-dimensional topography of the workpiece surface machined in Case 4, showing that the two-dimensional sine wave grid surface is very smooth. The surface roughness of the two-dimensional sine wave grid was less than 1 nm Sa. Fig. 20 (a) shows a microscope image of the machined surface observed by a differential contrast microscope. No crack appears on the machined surface. The SEM image of the cutting chips is shown in Fig. 20(b). Continuous chips were generated during the machining process, which are similar to the chips generated in ductile-mode machining of single-crystal silicon [27–29], indicating that ductile material removal was realized in this study.

Conclusions

A feedforward process flow for deterministic error compensation was proposed for STS turning of freeform surfaces. The process flow was based on comprehensive modeling of all major error factors and simulation/prediction of the resulting workpiece form errors. The effectiveness of the process flow was experimentally verified. The following conclusions were obtained.

(1) The error factors in STS turning can be classified into three categories: program-related, tool-related and process-related error factors.
(2) The program-related error occurs in cutting point distribution and tool trajectory interpolation steps. Through simulation and optimization of the methods for these steps, the form error can be suppressed below the targeted tolerance in the shortest machining time.
(3) The tool-related error depends on tool-workpiece alignment. The simulation of error generation enables identifying dominant error factors and rapid tool alignment in high accuracy.
(4) The process-related error is caused by machine table acceleration, which depends on the cutting conditions and the control system configuration of the machine tool used. By adjusting the gains of the control system according to surface geometry and cutting conditions, the follow-up error can be suppressed effectively despite of the machine tool kinetics.
(5) Through modeling and simulation, all major error factors can be compensated before machining, without the necessity of repetitive trial-and-error test cuts. A two-dimensional sine wave grid was successfully fabricated by a single cut on single-crystal silicon with form accuracy of 8 nm P–V and surface roughness of less than 1 nm Sa.
(6) The predicted values of form errors were in good agreement with the experimental results, demonstrating the applicability of the proposed process flow.

The proposed process flow not only improves the machined workpiece form accuracy, but also reduces the time for repetitive surface metrology. It can also avoid extra tool wear caused by the long total cutting distance in trial-and-error test cuts. It is expected that it will contribute greatly to the ultraprecision manufacturing of high-value added freeform optical products, and so on. As a future task, the reliability of the proposed methods will be further investigated by performing machining experiments for various kinds of free form surfaces.

Declaration of Competing Interest

The authors declare that they have no known competing financial interests or personal relationships that could have appeared to influence the work reported in this paper.

Acknowledgements

References

[1] Zhang Z, Yan J, Kuriyagawa T. Manufacturing technologies toward extreme precision. Int J Extrem Manuf 2019;1:022001.

[2] Fang FZ, Zhang XD, Weckenmann A, Zhang GX, Evans C. Manufacturing and measurement of freeform optics. CIRP Ann Manuf Technol 2013;62:823–46.

[3] De Chiffre L, Kunzmann H, Peggs GN, Lucca DA. Surfaces in precision engineering, microengineering and nanotechnology. CIRP Ann Manuf Technol 2003;52:561–77.

[4] Jiang X, Scott P, Whitehouse D. Freeform surface characterisation - a fresh strategy. CIRP Ann Manuf Technol 2007;56:553–6.

[5] Hansen HN, Carneiro K, Haitjema H, De Chiffre L. Dimensional micro and nano metrology. CIRP Ann Manuf Technol 2006;55:721–43.

[6] Weck M. Precision cutting processes for manufacturing of optical components. Proc SPIE Int Soc Opt Eng 2001;4440:145–51.

[7] Scheiding S, Yi AY, Gebhardt A, Loose R, Li L, Risse S, et al. Diamond milling or turning for the fabrication of micro lens arrays: comparing different diamond machining technologies. Proc. SPIE, Adv. Fabr. Technol. Micro/Nano Opt. Photonics IV. 7927 2011. 79270N-1–11.

[8] Yi AY, Li L. Design and fabrication of a microlens array by use of a slow tool servo. Opt Lett 2005;30:1707.

[9] Kim HS, Il Lee K, Lee KM, Bang YB. Fabrication of free-form surfaces using a long-stroke fast tool servo and corrective figuring with on-machine measurement. Int J Mach Tools Manuf 2009;49:991–7.

[10] Zhang X, Fang F, Yu L, Jiang L, Guo Y. Slow slide servo turning of compound eye lens. Opt Eng 2013;52:023401.

[11] Yin ZQ, Dai YF, Li SY, Guan CL, Tie GP. Fabrication of off-axis aspheric surfaces using a slow tool servo. Int J Mach Tools Manuf 2011;51:404–10.

[12] Mukaida M, Yan J. Fabrication of hexagonal microlens arrays on single-crystal silicon using the tool-servo driven segment turning method. Micromachines 2017; 8.

[13] Ramesh R, Mannan MA, Poo AN. Error compensation in machine tools - a review. Part I: geometric, cutting-force induced and fixture-dependent errors. Int J Mach Tools Manuf 2000;40:1235–56.

[14] Yu DP, Hong GS, Wong YS. Profile error compensation in fast tool servo diamond turning of micro-structured surfaces. Int J Mach Tools Manuf 2012;52:13–23.

[15] Dai Y, Guan C, Yin Z, Tie G, Chen H, Wang J. Tool decentration effect in slow tool servo diamond turning off-axis conic aspheric surface. 5th Int. Symp. Adv. Opt. Manuf. Test. Technol. Adv. Opt. Manuf. Technol. 7655 2010:76550P.

[16] Chen C-C, Huang C-Y, Peng W-J, Cheng Y-C, Yu Z-R, Hsu W-Y. Freeform surface machining error compensation method for ultra-precision slow tool servo diamond turning. Opt Manuf Test X 2013;8838:88380Y.

[17] Neo DWK, Kumar AS, Rahman M. A novel surface analytical model for cutting linearization error in fast tool/slow slide servo diamond turning. Precis Eng 2014; 38:849–60.

[18] Neo WK, Nadhan MD, Kumar AS, Rahman M. A novel method for profile error analysis of freeform surfaces in FTS/STS diamond turning. Key Eng Mater 2014; 625:101–7.

[19] Keong NW, Kumar AS, Rahman M. A novel method for layered tool path generation in the fast tool servo diamond turning of noncircular microstructural surfaces. Proc Inst Mech Eng Part B J Eng. Manuf 2013;227:210–9.

[20] Gao W, Araki T, Kiyono S, Okazaki Y, Yamanaka M. Precision nano-fabrication and evaluation of a large area sinusoidal grid surface for a surface encoder. Precis Eng 2003;27:289–98.

[21] Gao W, Tano M, Araki T, Kiyono S. Precision fabrication of a large-area sinusoidal surface using a fast-tool-servo technique - Improvement of local fabrication accuracy -. JSME Int. J Ser C Mech Syst Mach Elem Manuf 2007;49:1203–8.

[22] Yu DP, Hong GS, Wong YS. Integral sliding mode control for fast tool servo diamond turning of micro-structured surfaces. Int J Automation Technol 2011;5 (1):4–10.

[23] Yu DP, Gan SW, Wong YS, Hong GS, Rahman M, Yao J. Optimized tool path generation for fast tool servo diamond turning of micro-structured surfaces. Int J Adv Manuf Technol 2012;63:1137–52.

[24] Kim HS, Kim EJ. Feed-forward control of fast tool servo for real-time correction of spindle error in diamond turning of flat surfaces. Int J Mach Tools Manuf 2003;43: 1177–83.

[25] Roblee JW. Characteristics of systems that rapidly diamond turn non-rotationally symmetric surfaces. Proc JSPE Spring Meet 2005:791–2.

[26] Hashimoto T, Roblee JW. Development of ultra-precision freeform manufacturing by single point diamond turning process. Proc JSPE Spring Meet 2014:65–6.

[27] Yan J, Yoshino M, Kuriagawa T, Shirakashi T, Syoji K, Komanduri R. On the ductile machining of silicon for micro electro-mechanical systems (MEMS), opto-electronic and optical applications. Mater Sci Eng A 2001;297:230–4.

[28] Yan J, Syoji K, Kuriyagawa T, Suzuki H. Ductile regime turning at large tool feed. J Mater Process Technol 2002;121:363–72.

[29] Mukaida M, Yan J. Ductile machining of single-crystal silicon for microlens arrays by ultraprecision diamond turning using a slow tool servo. Int J Mach Tools & Manuf 2017;115:2–14.